

# Quasi-ballistic, nonequilibrium electron distribution in inhomogeneous semiconductor structures

Dan Csontos\* and Sergio E. Ulloa

*Department of Physics and Astronomy, and Nanoscale and Quantum Phenomena Institute, Ohio University, Athens, Ohio 45701, USA*

We report on a study of quasi-ballistic transport in deep submicron, inhomogeneous semiconductor structures, focusing on the analysis of signatures found in the full nonequilibrium electron distribution. We perform self-consistent numerical calculations of the Poisson-Boltzmann equations for a model  $n^+ - n^- - n^+$  GaAs structure and realistic, energy-dependent scattering. We show that, in general, the electron distribution displays significant, temperature dependent broadening and pronounced structure in the high-velocity tail of the distribution. The observed characteristics have a strong spatial dependence, related to the energy-dependence of the scattering, and the large inhomogeneous electric field variations in these systems. We show that in this quasi-ballistic regime, the high-velocity tail structure is due to pure ballistic transport, whereas the strong broadening is due to electron scattering within the channel, and at the source(drain) interfaces.

PACS numbers: 73.23.Ad, 72.15.Lh, 72.20.Ht, 73.40.Kp

As the downscaling of semiconductor devices has reached well into the deep submicrometer regime, the nonequilibrium nature of the carrier dynamics has become exceedingly important. In these systems, channel lengths comparable to the electron mean free path are possible at room temperature, and thus, ballistic and hot electron effects are expected to strongly influence the transport properties of modern devices. Although numerous studies of hot electron and ballistic transport have been performed,<sup>1</sup> there have been very few works on the microscopic carrier dynamics. It is, e.g., not clear how the details of the scattering at the channel interfaces, as well as within the channel, affect the ballistic nature of the transport, what the microscopic signatures of quasi-ballistic transport are, and how these issues are responsible for limiting the current in these systems.<sup>2,3</sup>

A comprehensive microscopic analysis of these issues requires the study of the electron distribution function, which is a challenging task, both experimentally and theoretically, due to the strongly nonequilibrium nature of the problem. There have been a few recent theoretical studies of ballistic MOSFETs<sup>2,4</sup> in which the electron distribution was obtained by solution of the Boltzmann Transport Equation (BTE) in the collisionless limit. In this pure ballistic limit, according to the models, the electron distribution within the channel is composed of near-equilibrium electron distributions in the contacts, and thus, due to the inhomogeneous self-consistent field, only displays an asymmetric, pronounced high-velocity peak, corresponding to ballistic electrons. In recent experimental studies on the other hand,<sup>5</sup> the electron distribution in submicron, inhomogeneous III-V systems was measured using Raman spectroscopy, and was shown to display strongly broadened velocity distributions and interesting high-velocity tail structure. It is clear that in realistic room-temperature devices, the electron scattering rate is finite and thus, a full solution of the BTE, including scattering is required. Such an analysis was in fact already initiated by Baranger and Wilkins.<sup>6</sup> These authors solved the

BTE self-consistently with the Poisson equation for  $n^+ - n^- - n^+$  GaAs structures, and found significantly out-of-equilibrium electron distributions in the channel region, and in particular, a high-velocity peak corresponding to ballistic electrons. However, the physical mechanisms of the strong broadening and the details of the electron distribution characteristics were not clearly resolved. In addition, the scattering introduced in the BTE was structureless, while the distribution function in inhomogeneous systems is strongly energy-dependent.

In this paper we present a numerical analysis of the nonequilibrium electron distribution in submicron, inhomogeneous semiconductor structures. We show that the electron distribution function has a highly nonequilibrium form, is significantly broadened, and displays interesting structure in the high-velocity tail. In addition, the observed features are spatially dependent and very sensitive to the inhomogeneous electric field, temperature and detailed characteristics of the scattering, where we find that an energy-dependent scattering process strongly affects the details of the electron distribution. In addition to providing insight to the general quasi-ballistic transport characteristics in the electron distribution of submicron structures, we believe that our results are relevant for the recently observed nonequilibrium velocity distributions observed in the recent experiments.

Our study is based on numerical analyses in which we explicitly calculate the 1D, steady-state electron velocity distribution function,  $f(x, v)$ , through a model  $n^+ - n^- - n^+$  GaAs structure.<sup>7</sup> We consider a nondegenerate system and use a numerical, self-consistent approach based on the coupled Poisson-Boltzmann equations, which enables us to capture essential nonequilibrium and inhomogeneous transport phenomena.<sup>8</sup> Scattering is treated within the relaxation-time approximation, using realistic, energy-dependent scattering rates corresponding to polar-optical phonon (POP) scattering, which is the dominating scattering mechanism in GaAs

at room temperature.<sup>9</sup> The POP scattering rate is given by<sup>10</sup>

$$\frac{1}{\tau_p(\varepsilon)} = \frac{e^2\omega_0\kappa}{2^{3/2}\pi\epsilon_0\hbar} \sqrt{\frac{m^*}{\varepsilon}} \left\{ n_0 \sinh^{-1} \left[ \frac{\varepsilon}{\hbar\omega_0} \right]^{1/2} + (n_0 + 1) \sinh^{-1} \left[ \frac{\varepsilon}{\hbar\omega_0} - 1 \right]^{1/2} \right\}, \quad (1)$$

where  $\kappa = (1/\epsilon_\infty - 1/\epsilon)$ ,  $\epsilon_\infty$  is the high-frequency dielectric constant,  $\epsilon$  is the static dielectric constant,  $\hbar\omega_0$  is the optical phonon energy and  $n_0 = [\exp(\hbar\omega_0/k_B T) - 1]^{-1}$  is the phonon occupation number. In Eq. (1) the first term corresponds to POP absorption and the second to POP emission, which only occurs when  $\varepsilon(p) > \hbar\omega_0$ .

In Fig. 1 we show the electron potential energy, electric field and distribution function at  $T = 300$  K, and  $V_b = -0.3$  V, for a 200 nm long lightly doped ( $10^{13}$  cm<sup>-3</sup>) GaAs slab sandwiched between two highly doped ( $10^{17}$  cm<sup>-3</sup>) long contacts. In order to highlight the effects of inhomogeneities and scattering while keeping the nature of the scattering *structureless*, we first use constant scattering times in our calculations (in Fig. 1,  $\tau_2 = 2.5 \cdot 10^{-13}$  s), and subsequently compare these results with realistic energy-dependent scattering times. For comparison, the potential energy and electric field at  $V_b = 0$  are plotted in Fig. 1(a) (dashed lines). Several direct observations can be made from the electrostatics depicted in Fig. 1(a). A potential barrier is formed in the  $n^-$  region due to the inhomogeneous doping profile that gives rise to the diffusion of electrons from the highly doped  $n^+$  into the lightly doped  $n^-$  region. Second, as a result, a strong electric field on the order of 10 kV/cm is formed within the device, even in the absence of an external field. Third, as a bias voltage is applied, a large portion of the voltage drop occurs over the submicron  $n^-$  region, giving rise to a strongly inhomogeneous field distribution, in contrast to the  $n^+$  contact regions, where the field in comparison is very low and constant.

In Fig. 1(b), the calculated normalized electron distribution function,  $f(x_i, v)v_{th}/n(x_i)$ , where  $v_{th}$  is the thermal velocity, is shown at different spatial points along the sample for the  $V_b = -0.3$  V case. At  $x_1 = -0.15$   $\mu\text{m}$ , the electrons injected from the source display a shifted MB distribution. This is expected throughout the highly-doped contact regions, where the field is constant and low ( $\approx 0.1$  kV/cm) and thus, the distribution function can be described by the linear response solution to the homogeneous BTE,  $f(x, v) = f_{MB}(x, v)[1 - veE(x)\tau/k_B T]$ . At  $x_2 = -0.07$   $\mu\text{m}$ , corresponding to the top of the potential barrier, the distribution is asymmetric, showing a suppression of electrons in the  $v < 0$  tail of the distribution. This is caused by the asymmetric potential barrier, which prevents left-moving electrons ( $v < 0$ ) to reach  $x_2$ . Deep in the  $n^-$  region, for  $x > x_2$ , the electron distribution displays a strong spatial dependence as well as significant broadening. To better understand the overall spatial dependence of the distribution function, Fig. 1(c)

shows the contour plot of  $f(x, v)$ , around the interesting  $n^-$  region. It is clear that the electron distribution in the  $n^-$  region displays a distinct peak that is rapidly shifted toward higher velocities for increasing  $x > x_2$ . This is a signature of *ballistic transport* and occurs due to the rapid and large (compared to  $k_B T$ ) potential energy drop<sup>2,4,6</sup> and corresponding strong inhomogeneous electric field. In addition to the ballistic peak, for increasing  $x > x_2$ , the electron distribution is broadened and a low-velocity contribution gradually builds up until the distribution is dominated by a low-velocity peak, see point  $x_5$  in Fig. 1(b) and the spatial dependence in Fig. 1(c). The origin of this broadening is two-fold: The thermionically injected electrons at  $x_2$ , with  $v > 0$ , are gradually thermalized at a rate  $1/\tau$  as they cross the channel, thus gradually “depopulating” the high-velocity peak

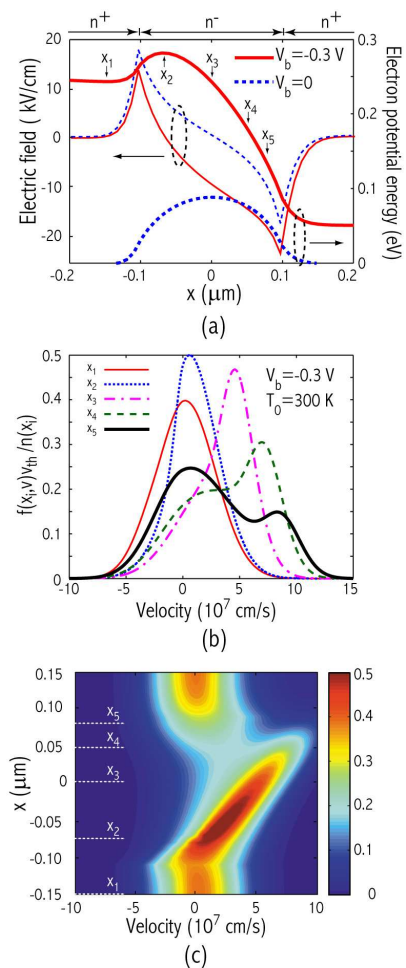


FIG. 1: (color online) (a) Electric field (thin lines) and potential energy (thick lines) profile for  $V_b = 0$  (dashed lines) and  $V_b = -0.3$  V (solid lines), (b) normalized electron distribution function calculated at the spatial points denoted by the arrows in (a), and (c) contour plot of  $f(x, v)v_{th}/n(x)$  around the  $n^-$  region for a  $n^+ - n^- - n^+$  GaAs structure with dimensions  $1.5/0.2/1.5$   $\mu\text{m}$  and doping profile  $10^{17}/10^{13}/10^{17}$  cm<sup>-3</sup>. Scattering time is  $\tau_2 = 2.5 \cdot 10^{-13}$  s.

corresponding to ballistic electrons. Second, electrons backscattered at the channel-drain interface, as well as injected electrons with  $v < 0$  from a near-equilibrium distribution in the drain, penetrate the channel with negative velocities, contributing to the negative and low-velocity end of the electron distribution. These electrons are scattered at a rate  $1/\tau$ , but also experience scattering at the steep potential energy barrier close to the source. Hence, close to the source and deep in the  $n^-$  region, the distribution is dominated by the ballistic peak corresponding to the source-injected ballistic electrons [see Fig. 1(b)]. Close to the drain, however, where the effective potential barrier is lower, the drain-injected and reflected electrons dominate the distribution and obscure the ballistic peak.

The spatial dependence of the electron velocity distribution is strongly influenced by the characteristics of the external and built-in fields, mobility, scattering mechanisms and temperature. In Fig. 2(a), (b) we show the distribution function calculated for the constant scattering times  $\tau_1 = 1.0 \cdot 10^{-13}$  s and  $\tau_3 = 4.5 \cdot 10^{-13}$  s, for the same structure and system parameters studied in Fig. 1 (with  $\tau_2 = 2.5 \cdot 10^{-13}$  s). While energy-independent, these scattering times correspond to realistic mobilities of GaAs. For the short scattering time,  $\tau_1 = 1.0 \cdot 10^{-13}$  s, the ballistic peak structure seen in Fig. 1(c) is significantly less pronounced and the average velocity of the electrons is strongly reduced. The latter observation is a natural consequence of the increase of the scattering rate. However, in addition, the fraction of the potential drop that occurs over the channel region also decreases with an increase in the scattering rate (not shown here) and hence, due to the decreased effective potential barrier, the drain-injected and reflected electrons penetrate deep into the channel. Therefore, the resulting distribution, although strongly out-of-equilibrium, does not display distinct ballistic features, but becomes broadened, asymmetric and shifted. For  $\tau_3 = 4.5 \cdot 10^{-13}$  s [Fig. 2(b)], the opposite effects are observed: A very distinct ballistic peak dominates the distribution function deep into the  $n^-$  region close to the drain, and less broadening is observed. This is due to an increase in the electron velocity given by the decreased scattering rate, and an increase in the effective potential barrier seen by electrons with  $v < 0$  coming from the drain.

In realistic systems, the scattering and relaxation processes can have a strong energy-dependence and thus, it is interesting to consider the effects of an energy-dependent scattering rate on the nonequilibrium distribution function. In Fig. 2(c) the energy-dependent POP scattering time  $\tau_p(\varepsilon)$ , calculated from Eq. (1) at  $T = 300$  K, is shown. For clarity, in the figure, we have also indicated the values of the constant scattering times used in the calculations shown in Figs. 2(a), (b) and 1(c). Below the *threshold* for POP emission, the scattering time is in the range  $\approx 3.5 - 4 \cdot 10^{-13}$  s, whereas above the threshold, the scattering time has a relatively weak de-

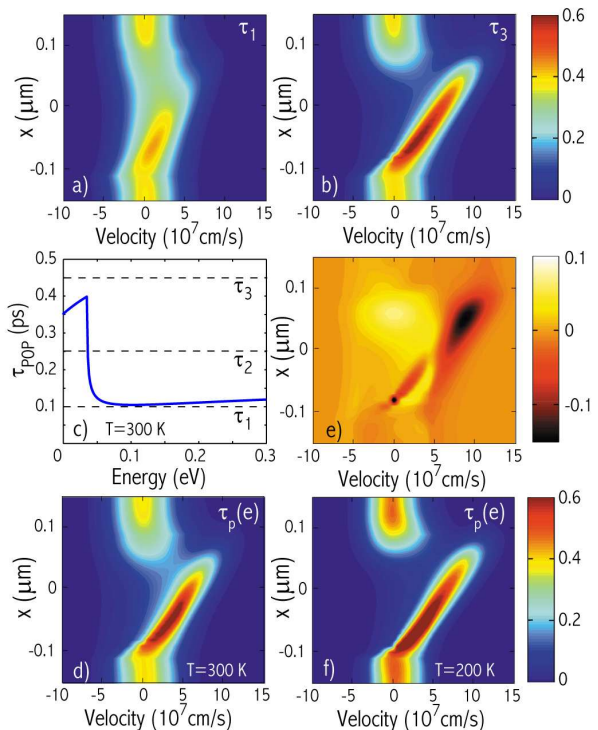


FIG. 2: (color online) Normalized distribution function,  $f(x, v)v_{th}/n(x)$ , for  $\tau_1 = 1.0 \cdot 10^{-13}$  s (a),  $\tau_3 = 4.5 \cdot 10^{-13}$  s (b),  $\tau_p(T = 300$  K) (d), and  $\tau_p(T = 200$  K) (f). (c) POP scattering time at  $T = 300$  K. (e) Difference between the normalized distribution functions calculated for  $\tau_p(T = 300$  K) and  $\tau_3$  [plots (d) and (b)].

pendence on energy (in this particular energy interval) and is close to  $\approx 1 \cdot 10^{-13}$  s. The corresponding electron distribution function, calculated at  $T = 300$  K is shown in Fig. 2(d). Strong signatures of quasi-ballistic transport are seen, i.e., formation of a ballistic peak that evolves toward higher velocities, similarly to the calculations performed with the constant, energy-independent scattering times, and significant broadening and low-velocity contributions due to the scattering processes discussed above. The details of the distribution function and its spatial dependence are, however, different. In Fig. 2(e), the difference between the normalized functions  $f[x, \tau_p(\varepsilon)]v_{th}/n(x) - f(x, \tau_3)v_{th}/n'(x)$  [ $n(x)$  and  $n'(x)$  are the electron densities corresponding to the two calculated distribution functions] is shown. The observed difference can be explained as follows: Electrons with velocities below  $v_{tp} \approx 4.3 \cdot 10^7$  cm/s, which corresponds to a kinetic energy comparable to the threshold for POP emission [Fig. 2(c)], have a large mean free path and behave ballistically, as concluded by the results shown by the calculations for  $\tau_3$  shown in Fig. 2(b). For electrons with higher kinetic energies on the other hand the scattering rate is higher and thus the electrons relax toward lower energies at an increasing rate. However, the picture is more complicated, since the detailed energy-dependence of the scattering effectively also changes the characteristics of

the inhomogeneous field due to the charge redistribution caused by the scattering.

Finally, we briefly discuss the effects of temperature, which is the parameter that, next to the applied electric field, is most easily tuned in experiments. In Fig. 2(f) we show the electron distribution calculated at  $T = 200$  K. Below the threshold for POP emission, the calculated scattering time (not shown here) is in the range  $\approx 8.2 - 9.2 \cdot 10^{-13}$  s, whereas above threshold, the scattering time has weak energy dependence and is  $\approx 1.5 \cdot 10^{-13}$  s. As anticipated from the above discussion, the main effects of lowering the temperature and, thus, increasing of the phonon scattering time, are: *i*) higher average velocities, *ii*) larger spatial extension of the ballistic peak, *iii*) narrowing of the ballistic peak in the  $n^-$  region as well as the diffusive peaks in the source/drain, and *iv*) suppression of the drain-injected electron contribution to the electron distribution in the channel region, due to an increase in the effective potential barrier.

In summary, we have studied the electron distribution in inhomogeneous, deep submicron semiconductor structures by self-consistent calculations of the semiclassical BTE. We have shown that the electron distribution

in general is strongly out-of-equilibrium, significantly broadened and displays pronounced structure in the high-velocity tail. These characteristics of quasi-ballistic transport are very sensitive to the energy-dependent scattering in the channel and at the source(drain) interface, as well as the strongly inhomogeneous electric field. Our results are similar to recent experimental observations.

*Note added after submission:* An interesting study of quasiballistic transport in nanoscale semiconductor structures with focus on the scattering and the mathematical nature of the BTE at the top of the potential energy barrier at the source-channel interface has been published very recently by Sano.<sup>11,12</sup> We note that although the calculations were done for completely different material (Si) and system parameters, the features of the distribution shown in Fig. 3 of Ref. 12 are similar to the features of the distributions calculated here, and are due to the mechanisms discussed in our paper.

This work was supported by the Indiana 21st Century Research and Technology Fund.

---

\* Electronic address: csontos@phy.ohiou.edu

<sup>1</sup> See, e.g., U. Ravaioli, *Semicond. Sci. Technol.* **13**, 1 (1998), and references therein.

<sup>2</sup> M. Lundstrom, and Z. Ren, *IEEE Trans. Electron Devices* **49**, 133 (2002).

<sup>3</sup> A. Svizhenko, and M. P. Anantram, *IEEE Trans. Electron Devices* **50**, 1459 (2003).

<sup>4</sup> J.-H. Rhew, Z. Ren, and M. S. Lundstrom, *Solid State Electronics* **46**, 1899 (2002).

<sup>5</sup> E. D. Grann *et al.*, *Phys. Rev. B* **51**, 1631 (1995); E. D. Grann *et al.*, *Phys. Rev. B* **53**, 9838 (1996); K. T. Tsen *et al.*, *Appl. Phys. Lett.* **69**, 3575 (1996); W. Liang *et al.*, *Appl. Phys. Lett.* **82**, 1413 (2003); W. Liang *et al.*, *Appl. Phys. Lett.* **84**, 3681 (2004).

<sup>6</sup> H. U. Baranger, and J. W. Wilkins, *Phys. Rev. B* **36**, 1487

(1987); H. U. Baranger, and J. W. Wilkins, *Phys. Rev. B* **30**, 7349 (1984).

<sup>7</sup> GaAs material parameters:  $m^* = 0.067m_0$ ,  $\epsilon = 13.1$ ,  $\epsilon_\infty = 10.92$ ,  $\hbar\omega_0 = 0.03536$  eV.

<sup>8</sup> D. Csontos and S. E. Ulloa, (to be published in *J. Comp. Electronics*). Also available at arXiv.org, cond-mat/0411499.

<sup>9</sup>  $e^- - e^-$  scattering, while possibly comparable to POP scattering in the  $n^+$  regions, is much weaker in the channel region due to the low doping ( $N_D = 10^{13}$  cm<sup>-3</sup>).

<sup>10</sup> B. R. Nag, *Theory of electrical transport in semiconductors* (Pergamon Press, Oxford, 1972).

<sup>11</sup> N. Sano, *Phys. Rev. Lett.* **93**, 246803 (2004).

<sup>12</sup> N. Sano, *Appl. Phys. Lett.* **85**, 4208 (2004).